An efficient multigrid FEM solution technique for incompressible flow with moving rigid bodies

Decheng Wan, Stefan Turek, and Liudmila S. Rivkind

Institute of Applied Mathematics LS III, University of Dortmund,
Vogelpothsweg 87, 44227 Dortmund, Germany

Summary. This paper uses the fictitious boundary method described in [1] for the solution of incompressible flow with moving rigid bodies in complex geometries. The method is based on a special treatment of Dirichlet boundary conditions inside of a FEM approach in the context of a hierarchical multigrid scheme such that the flow can be efficiently computed on a fixed computational mesh while the solid boundaries are allowed to move freely through the given mesh. In this paper, we focus on the calculations of the drag and lift forces acting on the moving solid bodies which are not captured by the mesh. The comparison between the present and benchmark results for the flow around a circular cylinder with different Reynolds numbers is first presented, and then the result for a circular cylinder oscillating in a channel is given. The simulation results compared with corresponding reference results are found to be very reasonable and satisfactory.

1 Introduction

Incompressible flow problems with moving rigid bodies in complex geometries have drawn attention of numerous investigators. Their studies have been motivated by the desire to understand the fundamental physics of such flows as well as their practical importance in various areas. The phenomena of such flow problems are visible everywhere around our living environments such as: flow around high-rise building, the drag force induced by driving car accelerating in the wind, ocean current interaction with the offshore structures, sedimentation flow in estuary and sand flow in desert, etc.

From the numerical point of view, incompressible flow with moving rigid bodies in complex geometries is quite hard to simulate, since it can require a huge amount of time for the generation or deformation of the computational grid when the corresponding boundaries are complex or changing. Such problems have motivated the development of numerous algorithms, which can be broadly classified into two families. One of them is a 'body-conformal approach' which always keeps the computational mesh in accordance to the geometrical details [2, 3]. Another one is a 'fixed grid approach' in which case the mesh is (arbitrarily) fixed and internal objects are allowed to move freely through the mesh [4, 5]. One big advantage of such 'fixed grid approaches' over the conventional 'body-conformal approaches' is that the computational mesh remains unchanged such that the CPU cost per time step can be significantly decreased - less computational effort due to saving the expensive mesh generation - and that such techniques can be easily incorporated into standard CFD codes which mostly allow fixed computational grids without local adaptivity only; however, the resulting accuracy is not clear. Therefore, the overall aim is to deal successfully with the moving boundaries such that the accuracy of the numerical approximation is sufficiently high while at the same time also the computational cost is decreased.

In the spirit of the 'fixed grid approaches', a simple and efficient 'fictitious boundary method' for the detailed simulation of incompressible flow with complex geometries and/or moving interfaces was developed in the paper [1]. The method is based on a fixed unstructured FEM background grid. It starts with a coarse mesh which contains already many of geometrical fine-scale details, and employs a (rough) boundary parametrization which sufficiently describes all large-scale structures with regard to the boundary conditions. Then, treat all fine-scale features as interior objects such that the corresponding components in all matrices and vectors are unknown degrees of freedom which are implicitely incorporated into all iterative solution steps (see [1]).

In this paper, we used the fictitious boundary method for the simulation of incompressible flow with moving rigid bodies in complex geometries. In many cases, the calculation of forces acting on the moving rigid bodies is very important for the further study of the interaction between fluid and body, like in particulate flow, sedimentation flow, and fluid-structure flow, etc. However, in the fictitious boundary method, it is not so easy and straightforward to compute these interesting forces, because the drag coefficient C_d and lift coefficient C_l acting on the moving solid bodies are a very delicate quantity: they include the results directly on the wall surface of the moving rigid bodies which is represented implicitly in the fictitious boundary method due to the use of a fixed grid rather than a body-conformal grid. Therefore, the integral of forces only over the wall surface of rigid bodies cannot be implemented directly in the fictitious boundary method. For overcoming this difficulty, a volume integral instead of the conventional surface integral for the calculation of the C_d and C_l by introducing an auxiliary function [7] or two additional functions [8] is suggested. Obviously, in such volume integral calculations, the reconstruction of the wall surface of the moving rigid bodies can be avoided. In this paper, we use the Duchanoy's idea of the volume integral [7], and expand his implementation in a finite volume method into the finite element method and the fictitious boundary method.

2 The fictitious boundary method

The details of the fictitious boundary method have been described in [1]. For the following considerations, let Ω be a bounded domain with a piecewise smooth boundary Γ. The equations to be solved are the incompressible Navier-Stokes equations

$$\rho \frac{\partial \mathbf{u}}{\partial t} + \rho \mathbf{u} \cdot \nabla \mathbf{u} = \mathbf{f} - \nabla p + \mu \nabla^2 \mathbf{u}\,, \qquad \nabla \cdot \mathbf{u} = 0\,, \tag{1}$$

where $\mathbf{u}$ is the velocity, p the pressure, μ the dynamic viscosity coefficient, ρ the density, $\mathbf{f}$ the source term which may include the gravitational force. The above equations are to be solved with $\mathbf{u}(\mathbf{x}, t) = \mathbf{u}_\partial(\mathbf{x}, t)$ on parts of the boundaries of the flow domain where $\mathbf{u}_\partial(\mathbf{x}, t)$ is the prescribed boundary velocity, including time-dependent moving boundaries. The details of solving such incompressible flow problems can be found in the FeatFlow software [10, 11] which is based on (nonconforming) FEM discretizations, adaptive implicit time-stepping, nonlinear Newton-like methods, (geometrical) multigrid solvers (for velocity and pressure separately) on quite arbitrary domains.

In the following part, we give the description of a volume integral approach for the calculation of the drag coefficient C_d and lift coefficient C_l acting on the moving solid bodies. Let S be the wall surface of the rigid bodies, $\mathbf{n}_S$ be the inward pointed unit

normal with respect to Ω and tangential vector $\tau = (n_y, -n_x)$. The drag and lift forces are usually calculated by a surface integral as follows

$$F_D = \int_S \left(\mu \frac{\partial \mathbf{u}_\tau}{\partial \mathbf{n}_S} n_y - p\, n_x \right) ds\,, \qquad F_L = -\int_S \left(\mu \frac{\partial \mathbf{u}_\tau}{\partial \mathbf{n}_S} n_x + p\, n_y \right) ds\,, \tag{2}$$

while the drag and lift coefficient are calculated via

$$C_d = \frac{2F_D}{\rho \bar{U}^2 D}\,, \qquad C_l = \frac{2F_L}{\rho \bar{U}^2 D}\,, \tag{3}$$

where $\bar{U}$ is the characteristic velocity, and D the characteristic length.

From Eq.(3) and Eq.(2), we can see that the surface integral around the wall surface of the rigid bodies should be conducted for the calculation of the C_d and C_l. However, in the present fictitious boundary method, the shapes of the wall surface of the moving rigid bodies is implicitly imposed in the fluid field. If we reconstruct the shapes of the wall surface of the moving rigid bodies, it is not only a time consuming work, but also the accuracy is only first order due to a piecewise constant interpolation. For overcoming this problem, we use the following method to calculate the C_d and C_l in which the surface integral is replaced by a volume integral. We define a parameter α as

$$\alpha(\mathbf{x}) = \begin{cases} 1 & \text{for} \quad \mathbf{x} \in \Omega_c\,, \\ 0 & \text{for} \quad \mathbf{x} \in \Omega\,, \end{cases} \tag{4}$$

where $\mathbf{x}$ denotes the coordinates of the edge midpoints of cells, Ω_c is the domain occupied by the rigid bodies, Ω is the fluid domain, the whole domain is $\Omega_T = \Omega \cup \Omega_c$. The importance of such a definition of the parameter can be seen from the fact that the gradient of α is zero everywhere except at the wall surface of the rigid bodies, and equal to the normal vector $\mathbf{n}$ defined on the grid [7, 12], i.e.

$$\mathbf{n} = -\nabla \alpha\,. \tag{5}$$

The total stress tensor σ of the fluid flow is

$$\sigma = -p\mathbf{I} + \mu \left[\nabla \mathbf{u} + (\nabla \mathbf{u})^T \right]\,. \tag{6}$$

Hence the forces acting over the wall surface of the rigid bodies can be computed by

$$\mathbf{F}_T = \int_{\Omega_T} \sigma\, \mathbf{n}\, d\Omega = -\int_{\Omega_T} \sigma\, \nabla \alpha\, d\Omega\,. \tag{7}$$

The drag force and lift force can be obtained from the Eq.(7),

$$F_D = -\int_{\Omega_T} \left[\mu \left(\frac{\partial u}{\partial x} \frac{\partial \alpha}{\partial x} + \frac{\partial u}{\partial y} \frac{\partial \alpha}{\partial y} \right) - p \frac{\partial \alpha}{\partial x} \right] d\Omega\,, \tag{8}$$

$$F_L = -\int_{\Omega_T} \left[\mu \left(\frac{\partial v}{\partial x} \frac{\partial \alpha}{\partial x} + \frac{\partial v}{\partial y} \frac{\partial \alpha}{\partial y} \right) - p \frac{\partial \alpha}{\partial y} \right] d\Omega\,. \tag{9}$$

Therefore through Eq.(8), Eq.(9) and Eq.(3) we can calculate the new drag and lift coefficients (C_d and C_l) via the volume integral over the whole domain Ω_T instead of the surface integral over the wall surface of the rigid bodies in Eq.(2). The integral over

each element covering the whole domain Ω_T is evaluated with the standard 3×3 point Gaussian quadrature. Since the gradient $\nabla\alpha$ is non-zero only at the wall surface of the rigid bodies, thus the volume integrals need to be computed only in one layer of mesh cells around the rigid bodies. It is convenient for the present fictitious boundary method to calculate the C_d and C_l.

3 Numerical tests

This section consists of two parts. The first part presents a quantitative examination for the benchmark case of flow around a circular cylinder with $Re = 20$ and 100 solved by the present fictitious boundary method. The second part gives the computing results for a circular cylinder oscillating in a channel. For comparison, corresponding reference results are also presented.

3.1 Flow around a circular cylinder

We consider the benchmark case of flow around a circular cylinder described in the paper [9]. The body-conformal mesh of Fig. 1 (a) is used to provide reference results, while the channel meshes of Fig. 1 (b) and (c) are employed by the present fictitious boundary method. The channel height is $H = 0.41$ m, the cylinder diameter $D = 0.1$ m. The Reynolds number is defined by $Re = \bar{U}D/\nu$ with the mean velocity $\bar{U} = 2U(0,\, H/2,\, t)/3$. The kinematic viscosity of the fluid is given by $\nu = \mu/\rho = 10^{-3}\, m^2/s$ and its density by $\rho = 1\, kg/m^3$. The inflow profiles are parabolic with different U such that the resulting Reynolds numbers are $Re = 20$ (steady case) and $Re = 100$ (nonsteady case).

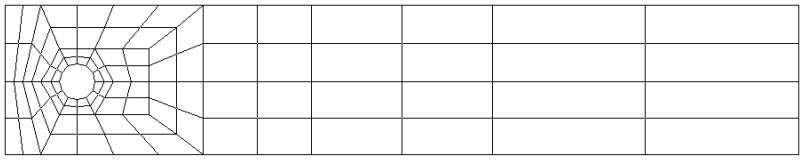

(a) body-conformal mesh (LEVEL = 2)

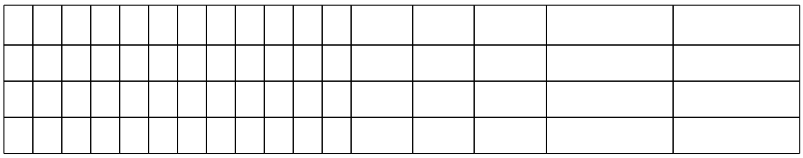

(b) channel mesh I (LEVEL = 1)

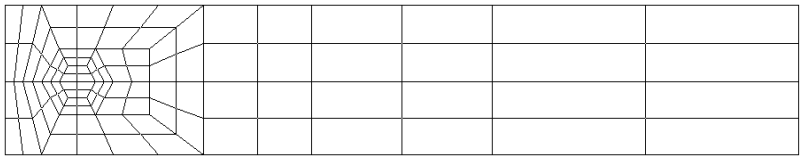

(c) channel mesh II (LEVEL = 2)

Fig. 1. Different coarse meshes

Table 1. The number of elements for different refined meshes

LEVEL	3	4	5	6	7
body-conformal mesh	384	1536	6144	24576	98304
channel mesh I	1088	4352	17408	69632	278528
channel mesh II	416	1664	6656	26624	106496

We first perform a stationary simulation ($Re = 20$), based on the body-conformal mesh, the channel mesh I and the channel mesh II, respectively. The shown coarse meshes will be successively refined by connecting opposite midpoints. Table 1 gives the number of elements for these meshes after such global refinements. Here LEVEL corresponds to the number of refinements. The following Table 2 shows the comparison of the drag coefficient C_d and the lift coefficient C_l based on the body-conformal mesh, the channel mesh I and the channel mesh II, respectively. The calculation of C_d and C_l based on the body-conformal mesh uses the surface integral formula in Eq.(2) which is referred as reference results, while for the cases of using the channel mesh I and the channel mesh II, the volume integral formula in Eq.(8) and Eq.(9) are employed. In this table, the results calculated from LEVEL = 3 to LEVEL = 7 are all shown together. The corresponding benchmark values in [9] are also listed in the table. From the comparisons, it can be seen that the results calculated by the present fictitious boundary method agree sufficiently well ($\sim 1\%$) with both the reference results. The results for the channel mesh I are found to be not completely satisfying, while the results for channel mesh II are improved since there is local refinement of the mesh near the wall surface of the cylinder. The results for such low Reynolds number simulations show that an appropriate global grid refinement as well as adequate local mesh adaptation are necessary. The present fictitious boundary method proves to be competitive with the standard approaches for such typical CFD applications.

Table 2. Comparison of C_d and C_l for $Re = 20$

	C_d			C_l		
LEVEL	Ref.	ch. mesh I	ch. mesh II	Ref.	ch. mesh I	ch. mesh II
3	0.53450D+01	0.55296D+01	0.54196D+01	0.56128D-02	0.12165D-01	0.24435D-02
4	0.55066D+01	0.53537D+01	0.54207D+01	0.84683D-02	0.10742D-01	0.67612D-02
5	0.55404D+01	0.54278D+01	0.55161D+01	0.98915D-02	0.61455D-02	0.89128D-02
6	0.55581D+01	0.55012D+01	0.55571D+01	0.10384D-01	0.99024D-02	0.94709D-02
7	0.55683D+01	0.55421D+01	0.55640D+01	0.10554D-01	0.97706D-02	0.10192D-01
Ref. [9]	0.55795D+01			0.10618D-01		

Next, we further examine the resulting accuracy for a medium range Reynolds number $Re = 100$ which leads to periodical time-dependent vortex shedding behind the cylinder. Since we are mainly interested in the spatial accuracy of the fictitious boundary method, in particular capturing the important effects near the cylinder, we try to eliminate the temporal discretization error by choosing very small time steps. Then, we proceed the nonstationary simulations until a fully periodical flow behaviour of all quantities has been observed. Finally, we compare the results for one period. Figure 2 shows the results of

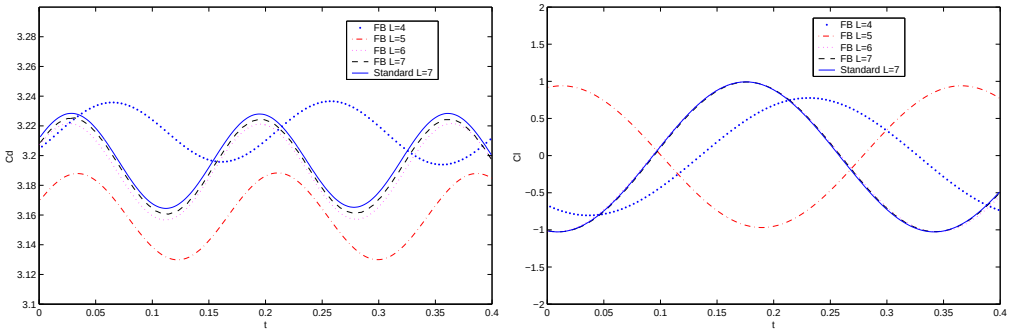

Fig. 2. Periodical results of C_d and C_l for $Re = 100$

the C_d and C_l. The "Standard $L = 7$" means that the body-conformal mesh of Fig. 1 (a) with 7 level refinement was used to provide the reference result, while "FB $L = 3 \sim 7$" represents the results obtained by the present fictitious boundary method using the channel mesh I in Fig. 1 (b) with different refinement levels. From these figures, we can see that the various results are identical with regard to the reference results. The results also show that the present fictitious boundary method leads to comparative results like the standard approaches with 'body-fitted' meshes. It can also be claimed that results with higher accuracy can be reached via local mesh adaptivity (see for example the concept of aligned adaptive computational meshes in [1]).

3.2 An oscillating cylinder in a channel

To demonstrate the ability of the present fictitious boundary method to handle flows with complex moving boundaries, we have chosen a flow configuration with a cylinder undergoing sinusoidal transverse oscillation in a channel with specified amplitudes and frequencies. The channel mesh of Fig. 3 (a) is employed by the present fictitious boundary method. The computational domain size is (2.2×0.41). The mean location of the cylinder center (X_0, Y_0) is $(1.1, 0.2)$ relative to the left bottom corner of the domain. The cylinder diameter D is equal to 0.1. No-slip is prescribed on the left, right, top and bottom boundaries. The cylinder is oscillating sinusoidally such that the location of its center (X_c, Y_c) is given by $(X_c(t) = X_0 + A\sin(2\pi f\, t),\ Y_c(t) = Y_0)$, where t is the time, and $A = 0.25$ and $f = 0.25$ are amplitude and frequency of the oscillation, respectively. The kinematic viscosity of the fluid is given by $\nu = \mu/\rho = 10^{-3}\, m^2/s$ and its density by $\rho = 1\, kg/m^3$. The fluid in channel is initially at rest. Since there is no benchmark result available for comparison, we carried out a reference calculation to provide comparing data. In the reference calculation, the body-conformal mesh of Fig. 3 (b) is used, we fix the cylinder but set the coordinate system moving with the same motion but with opposite moving direction of the moving cylinder in the calculation of the fictitious boundary method. Table 3 gives the number of elements for the channel mesh and body-conformal mesh in Fig. 3 with different numbers of refined levels.

Fig. 4 gives contour plots for the vorticity distribution obtained by the fictitious boundary method based on the channel mesh. These pictures show that the flow in the channel is disturbed by the oscillating cylinder, and the vortex is generated periodically in the wake of the cylinder. The range of wakes becomes longest when the cylinder is at the end of the moving direction ($t = t_0 + \frac{1}{4}T$, $t_0 + \frac{3}{4}T$, T is time period), while when the

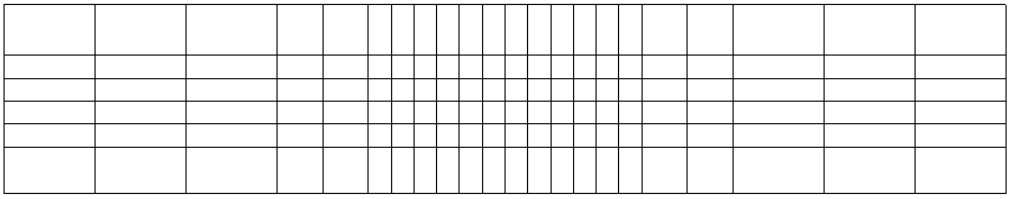

(a) channel mesh (LEVEL = 1)

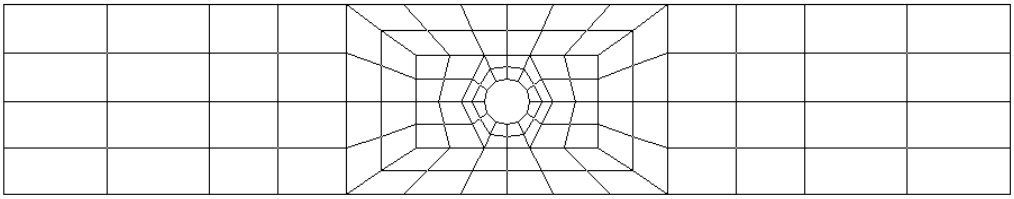

(b) body-conformal mesh (LEVEL = 2)

Fig. 3. Coarse meshes used for the oscillating cylinder in a channel

cylinder is in the middle position of its oscillation, the flow is seriously perturbed and becomes more complex ($t = t_0$, $t_0 + \frac{2}{4}T$). Fig. 5 illustrates the comparison of the drag coefficient C_d and lift coefficient C_l between the results of the fictitious boundary method based on the channel mesh and the reference calculation based on the body-conformal mesh. The results calculated from LEVEL = 4 to LEVEL = 7 are all shown together. The corresponding coefficients C_d and C_l for one period between $t = 19.79$ to 23.79 are shown in Fig. 5 (c) and (f), the solid line represents the results of the reference calculation based on the body-conformal mesh at LEVEL = 7, while the dash line denotes the results obtained by the fictitious boundary method based on the channel mesh at LEVEL = 7. From the comparisons, we can see that both FB and Ref. results are identical with the increase of the mesh refinements. The FB results calculated by the present fictitious boundary method are agreeable very well with the reference results, although the FB results exhibit small oscillations due to the non-aligned cylinder movement through the grid lines.

Table 3. The number of elements for different refined meshes

LEVEL	4	5	6	7
channel mesh	8448	33792	135168	540672
body-conformal mesh	1792	7168	28672	114688

4 Conclusions

The presented fictitious boundary method for simulating incompressible flows with moving rigid bodies in complex geometries has been validated in a two-dimensional configuration. We showed that the use of an arbitrarily fixed (unstructured) FEM background

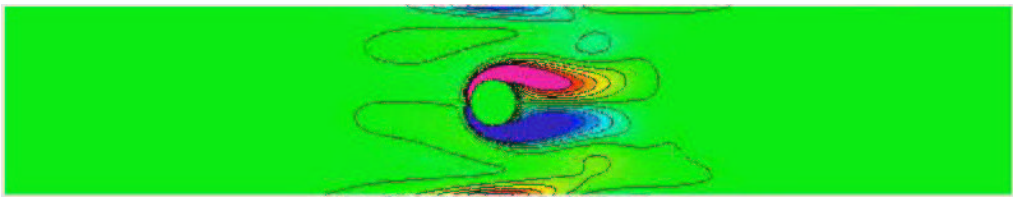

(a) $t = t_0$

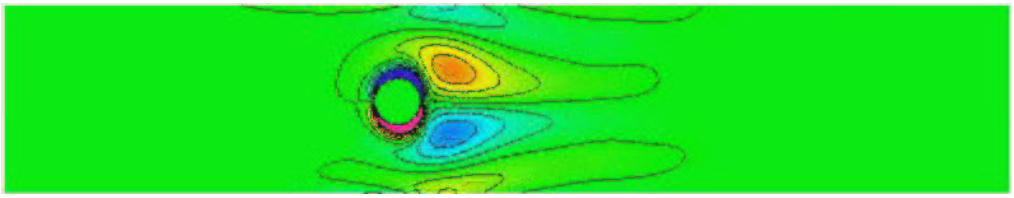

(b) $t = t_0 + \frac{1}{4}T$

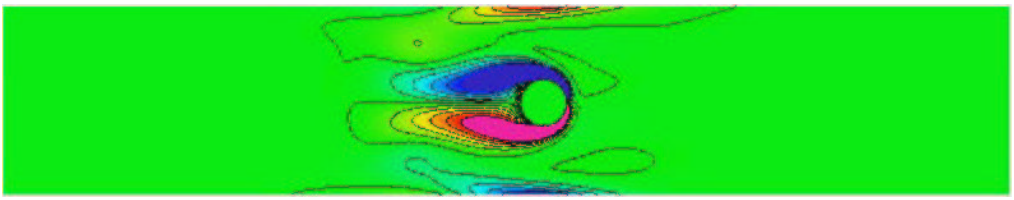

(c) $t = t_0 + \frac{2}{4}T$

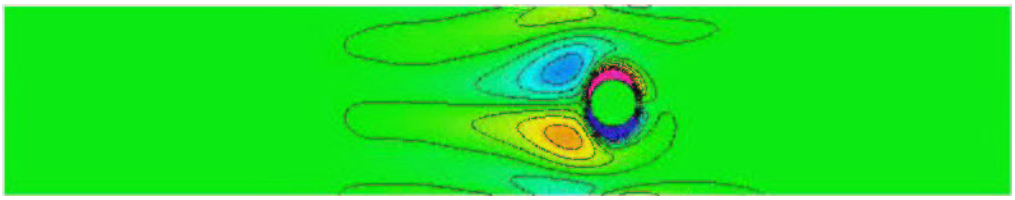

(d) $t = t_0 + \frac{3}{4}T$

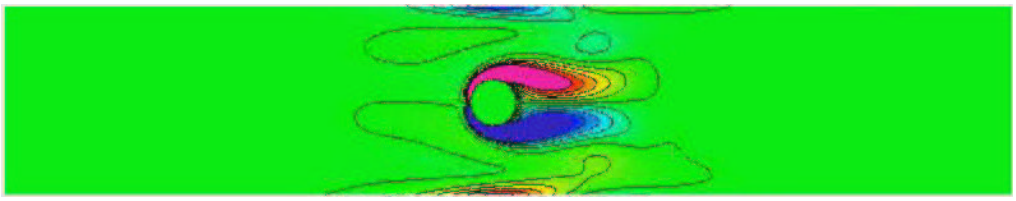

(e) $t = t_0 + T$

Fig. 4. Vorticity contour plot for an oscillating cylinder in a channel

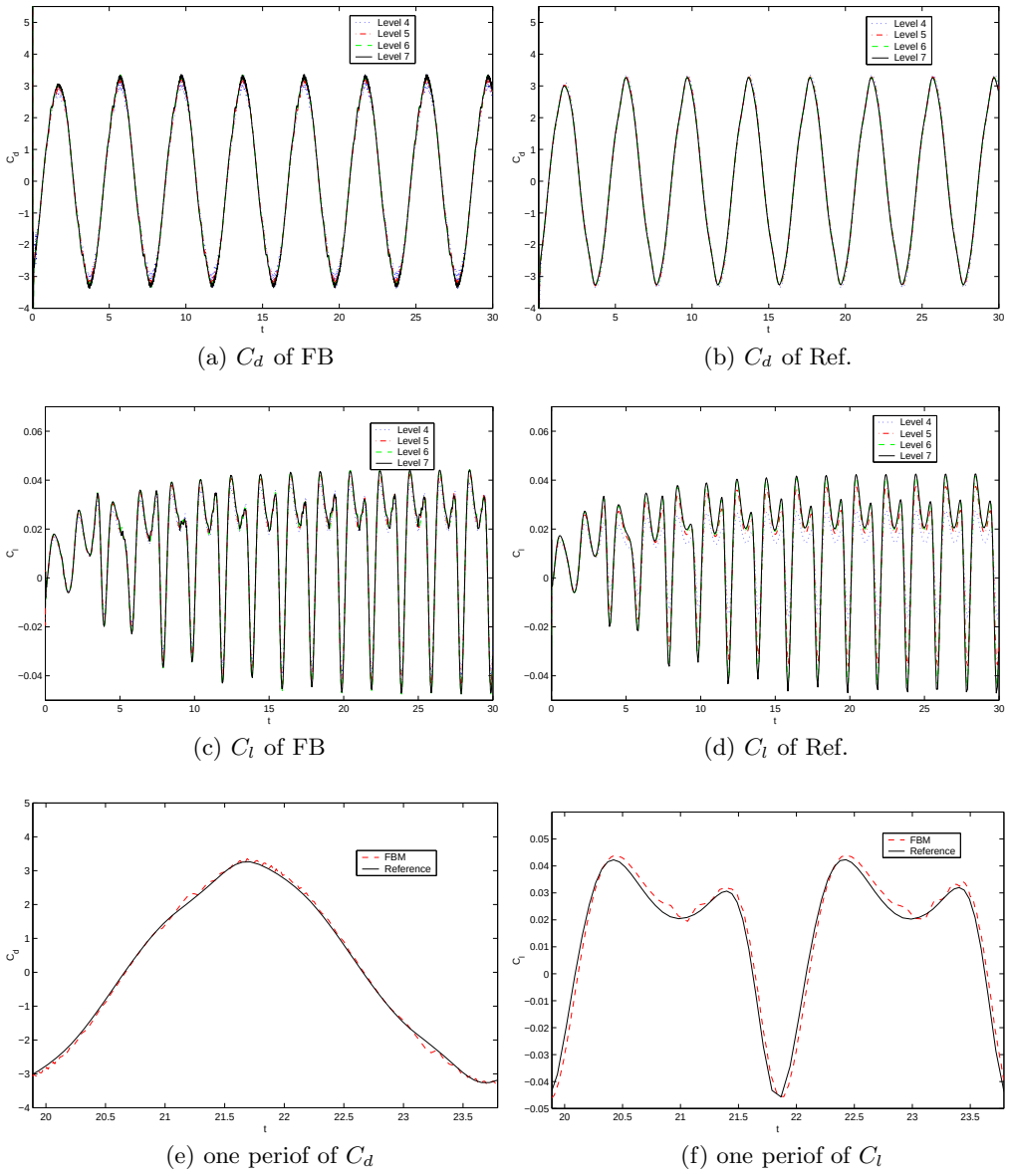

(a) C_d of FB (b) C_d of Ref.

(c) C_l of FB (d) C_l of Ref.

(e) one periof of C_d (f) one periof of C_l

Fig. 5. The comparison of C_d and C_l between fictitious boundary (FB) and reference (Ref.)

mesh is accurate enough to calculate those sensitive quantities (drag coefficient and lift coefficient) on the wall surface of the cylinder . Comparisons of the results using a body-fitted mesh and a fixed structured mesh show good agreement. The advantage of the present method is that since the body motion is independent of the mesh, problems associated with mesh reconfiguration and motion are avoided, computations on a fixed grid are cheaper than on a body-fitted one, and finally, the extension of the method to 3D is straightforward. It is also worthy to note that the availability of the present method to accurately compute the forces acting on the moving rigid bodies provides a good and

solid base for further study of particulate flow as well as the interaction between fluid and structure as proposed by Glowinski in the paper [4].

References

1. Turek, S., Wan, D.C. and Rivkind, L.S.: The Fictitious Boundary Method for the implicit treatment of Dirichlet boundary conditions with applications to incompressible flow simulations. Lecture Notes in Computational Science and Engineering, Volume 35, Springer Verlag, (2003)
2. Feng, J., Hu, H.H and Joseph, D.D.: Direct simulation of initial value problems for the motion of solid bodies in a Newtonian fluid; part 2, Couette and Poiseuille flows. J. Fluid Mesh. **277** (1994) 271
3. Hu, H.H.: Direct simulation of flows of solid-liquid mixtures. Int. J. Multiphase Flow. **22** (2) (1996) 335
4. Glowinski, R., Pan, T.W., Hesla, T.I. and Periaux, J.: A fictitious domain approach to the direct numerical simulation of incompressible viscous flow past moving rigid bodies: application to particulate flow. J. Comput. Phys. **169** (2001) 363
5. Glowinski, R.: Handbook of numerical analysis (Volume IX): Numerical methods for fluids (Part 3). Ciarlet, P.G and Lions, J.L. editors, North-Holland, (2003)
6. Heywood, J., Rannacher, R. and Turek, S.: Artificial boundaries and flux and pressure conditions for the incompressible Navier–Stokes equations. Int. J. Numer. Meth. Fluids **22** (1996) 325
7. Duchanoy, C. and Jongen, T.R.G.: Efficient simulation of liquid-solid flows with high solids fraction in complex geometries. Compters and Fluids **32** (2003) 1453
8. John, V.: Higher order finite element methods and multigrid solvers in a benchmark problem for the 3D Navier-Stokes equations. Int. J. Num. Meth. Fluids **40** (2002) 775
9. Schäfer, M. and Turek, S.: Benchmark computations of laminar flow around cylinder. in E.H. Hirschel (editor) Flow Simulation with High-Performance Computers II. Volume 52 of Notes on Numerical Fluid Mechanics, Vieweg (1996) 547
10. Turek, S.: Efficient Solvers for Incompressible Flow Problems. Springer Verlag, Berlin-Heidelberg-New York (1999)
11. Turek, S. et al.: **FEATFLOW** . Finite element software for the incompressible Navier–Stokes equations: User Manual, Release 1.2 (1999) (www.featflow.de)
12. Brackbill, J.U., Kothe, D.B. and Zemach, C.: A continuum method for modelling surface tension. J. Comput. Phys. **100** (1992) 335